JOURNAL OF MATERIALS SCIENCE 26 (1991) 2173–2183

Rheological behaviour and modelling of semi-solid Sn–15% Pb alloy

L. S. TURNG*, K. K. WANG
Sibley School of Mechanical and Aerospace Engineering, Cornell University, Ithaca, NY 14853, USA

The rheological behaviour and modelling of a semi-solid, Sn–15% Pb alloy characterized by a special coaxial-cylinder rheometer over a wide range of process conditions is reported. In particular, the effect of shear rate ($\dot{\gamma}$), volume fraction of solid (f_s), and cooling rate on the apparent viscosity (η) of the semi-solid Sn–15% Pb alloy under isothermal and various cooling conditions was studied. Based on the experimental data, the shear rate used in preparing the semi-solid alloy as well as the volume fraction of solid have the most dominant effects on the rheological properties of the semi-solid Sn–15% Pb alloy. A viscosity model expressed as $\eta(\dot{\gamma}, f_s) = (1 - f_s/f_s^*)^{-m(\dot{\gamma})}\, \eta_\infty(f_s)\{1 + [\dot{\gamma}^*(f_s)/\dot{\gamma}]^a\}^{n/a}$ is proposed in which f_s^* is the critical solid fraction at which the apparent viscosity goes to infinity, $\eta_\infty(f_s)$ corresponds to the asymptotic viscosity at infinity shear rate, and $\dot{\gamma}^*(f_s)$ characterizes the transition shear rate between the power-law and Newtonian regions. Finally, measurements with a differential scanning calorimeter were made and used to correlate the temperature and volume fraction of solid which, in turn, was corroborated with available data from the literature.

1. Introduction

When metal alloys are vigorously agitated during the early stage of solidification, the normally occurring dendritic structure is transformed into a system of nearly spherical solid particles suspended in a liquid matrix. Utilization of such slurries, so-called semi-solid alloys, in the high-pressure die-casting process has inherent advantages over superheated molten metals as discussed previously [1]. In particular, owing to its large and controllable viscosity, the semi-solid alloy can fill the die cavity in a progressive flow pattern, thus reducing the gas porosity frequently caused by the turbulent flow of a fully liquid metal. Such viscous flow behaviour of the semi-solid alloy not only ensures sound casting, but also greatly simplifies the task of mathematical modelling which might be used to predict the casting behaviour and thereby improve the casting quality.

Since the utilization of semi-solid alloys in casting applications was originally proposed [2–4], considerable effort has been directed towards characterizing the rheological behaviour of such materials [4–11]. In general, qualitative observations and empirical equations derived from experimental results have been reported for a number of semi-solid alloys under various process conditions. However, there is a definite need for a rheological model which can be incorporated into the mathematical modelling for a practical process such as the die casting of semi-solid alloys. The present work is intended to supplement the earlier pioneering investigations by placing emphasis on developing a rheological model suitable for modelling various metal-forming processes involving solidification such as the high-pressure die-casting process.

In this paper, an empirical viscosity model is proposed based on the characterization of a semi-solid, Sn–15% Pb alloy over a wide range of processing conditions. This model has been implemented into the numerical simulation of the fluidity test. The qualitative agreement between the present numerical predictions and the experimental data from [12] for other alloy system tends to confirm the predictive capability of the present model and its applicability to other semi-solid alloys [13]. In addition, work has also been done by employing a differential scanning calorimeter (DSC) to correlate the volume fraction of solid with temperature.

2. Experimental procedure and results

In order to characterize the rheological behaviour of a semi-solid, Sn–15% Pb alloy under a controllable environment, a dual-function, semi-solid-alloy producer and rheometer was fabricated, as shown in Fig. 1. Normally, this apparatus is a coaxial-cylinder rheometer with a conical end as initially proposed by Mooney and Ewart [14]. With such a configuration, the rate of shear in the cylindrical annulus and in the end zone is approximately the same, thus improving the uniformity of the microstructure and rheological properties of the resulting semi-solid alloy. The diameters of the inner and outer cylinders were 53.3 and 55.9 mm, respectively, with their lengths being 190.5 mm. However, if the inner cylinder is replaced

* *Present address*: AC Technology, Inc, Ithaca, NY 14850, USA.

0022–2461/91 $03.00 + .12

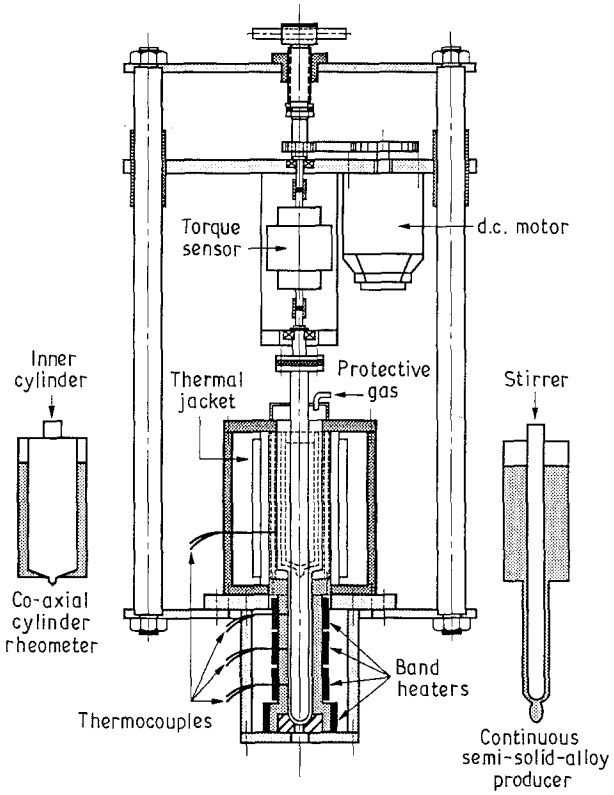

Figure 1 Schematic illustration of the experimental apparatus for the semi-solid-alloy producer and rheometer.

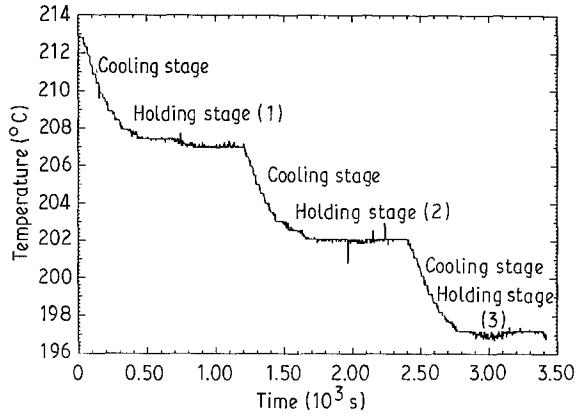

Figure 2 Temperature trace for semi-solid Sn–15% Pb alloy during cooling with three isothermal stages.

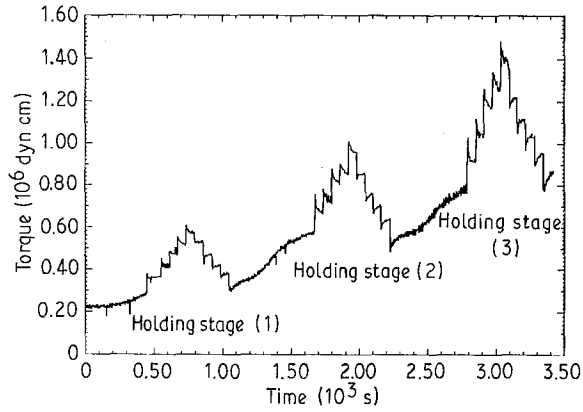

Figure 3 Torque measurement of semi-solid Sn–15% Pb alloy undergoing temperature trace in Fig. 2.

with a stirrer and a mixing chamber is added under the outer cylinder, this apparatus is readily changed from a coaxial-cylinder rheometer to a continuous semi-solid-alloy producer which can be used for casting experiments.

The thermal jacket, which is connected with a heating bath/circulator, as well as the cartridge heaters embedded in the wall of the outer cylinder, provide the desired controlled temperature trace (normally within $\pm$ 0.5 °C). A variable-speed d.c. motor and a speed controller are used to produce the shear with a rotary-transformer torque sensor measuring the required torque.

Basically, the rheological-characterization experiments performed in this study can be classified into two major categories, namely, isothermally held steady-state experiments and continuously cooled transient experiments. In the former case, the steady-state apparent viscosity is measured as a function of shear rate and solid fraction for the semi-solid Sn–15% Pb alloy at a fixed temperature. In the latter case, the variation of the apparent viscosity is investigated for the continuously cooled slurry under different cooling and shear rates.

2.1. The isothermal holding experiments

In this type of experiment, the Sn–15% Pb alloy is initially heated to a temperature above the liquidus and then slowly cooled down to a pre-set temperature at which it is then held isothermally. In this study, each experiment consists of one to four of such isothermal holding stages interspersed with cooling stages. Shown in Fig. 2 is a typical temperature trace with three clearly distinguishable isothermal holding stages pre-set at 207, 202, and 197 °C, respectively. During the cooling stages, the material is continuously agitated at a constant prescribed "initial" shear rate until the isothermal holding stage, when it is subjected to stepwise changes in shear rate at a fixed temperature. For example, Fig. 3 shows the torque measurement as a function of time corresponding to when the slurry was undergoing the aforementioned temperature change. An exploded view with detailed torque measurement along with corresponding shear rate for the second isothermal holding stage (at a temperature of 202 °C) are shown in Fig. 4. As is clearly seen, the shear rate is first increased in steps from the initial shear rate used in the previous cooling stage to a maximum value and then changed back to its initial value before another cooling process follows. In addition, for each step increase in shear rate, the torque increases initially with a sudden jump and then gradually decreases to a steady-state value. This phenomenon reverses when the shear rate is reduced. In rheology, such a time-dependent behaviour is typically associated with thixotropic materials whose structure and viscosity are both shear rate and time dependent. It has been found that at low shear rates the semi-solid alloy is made up of aggregates with a solid fraction which is effectively larger than its actual value due to the presence of entrapped liquid within the solid phase [5]. With increasing shear rates, the strong convection of flow breaks down the aggregates into smaller particles with less entrapped liquid, thus

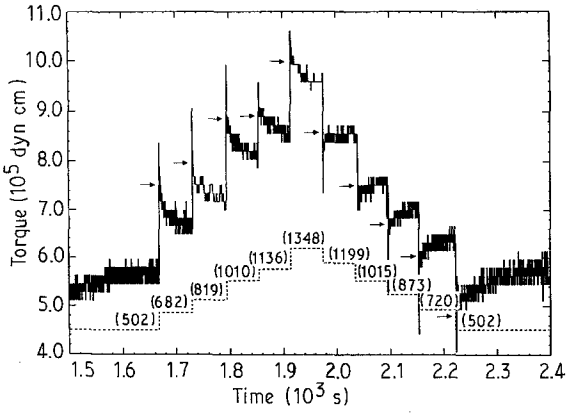

Figure 4 (——) Detailed torque measurement corresponding to the second isothermal holding stage shown in Fig. 3. Numbers shown in the parentheses indicate the imposed shear rates (s^{-1}) (– – –), whereas arrows indicate the required torque based on the viscosity immediately before the abrupt change in shear rate.

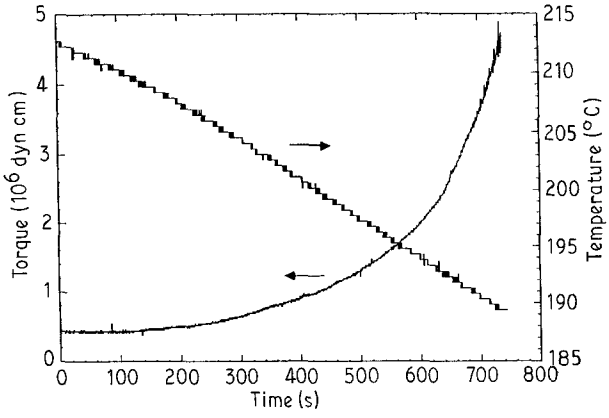

Figure 5 Temperature trace and corresponding torque measurement of semi-solid Sn–15% Pb alloy during slow continuous-cooling experiment with constant shear rate of 981 s^{-1}.

reducing the viscosity of the semi-solid alloy. A close examination of the experimental data also shows that the abrupt change in the torque measurement is essentially directly proportional to the change in shear rate, indicating little initial change in the apparent viscosity. In other words, the "overshoot" and "undershoot" in the torque measurement arise from the fact that the viscosity of the semi-solid Sn–15% Pb alloy immediately after the change in shear rate tends to remain the same as before the change. As a first step toward developing a constitutive model, the steady-state apparent viscosity, calculated from the torque measurement and rotating speed, as a function of shear rate and temperature (or, equivalently, solid fraction) will be employed to construct a viscosity model which will be discussed later.

2.2. The continuous-cooling experiments

In this type of experiment, the material is also initially heated to a temperature above the liquidus but then continuously cooled down into the solidification range. According to the rate of cooling, however, such continuous-cooling experiments can be further divided into three different kinds, namely slow cooling, fast cooling, and two-step cooling. For most of the continuous-cooling experiments, the shear rate exerted on the sample was held constant except for some two-step cooling experiments where some variations in shear rate were imposed.

A representative plot of the temperature trace and the corresponding torque history for a slow-cooling experiment are shown in Fig. 5. It can be seen that before the temperature drops below the liquidus (211 °C) at a time of approximately 100 s, the apparent viscosity of the Sn–15% Pb alloy basically remains constant as indicated by the constant torque during this period. Thereafter, the torque starts to increase due to the onset of solid particles. Akin to many conventional suspension systems, the torque measurement initially increases slowly and then more rapidly as more solid particles are produced and their interaction becomes more significant. Finally, when the temperature drops below 190 °C (at about 730 s), large fluctuations in torque begin to occur. Such a phenomenon has also been observed for other suspension systems (see, e.g. [15]). This apparently occurs when the volume fraction of solid is sufficiently large that some particle agglomerates may span the entire gap thickness between the cylinders, thus requiring additional torque to fragment them in order to maintain a constant shearing rate.

The fast-cooling experiment is basically the same as the slow-cooling experiment, in that the agitating shear rate is kept constant throughout the experiment. However, a much faster cooling rate is achieved by pumping oil at room temperature into the thermal jacket of the rheometer. A typical plot of the temperature trace as well as the corresponding torque history for the fast-cooling experiment are shown in Fig. 6. It can be seen that the resulting torque measurement is analogous to that of the slow-cooling experiment except that the cooling rate over the solidification range is about ten times faster.

Finally, the two-step cooling experiment is a combination of the slow- and fast-cooling experiments. To be more specific, reference is made to Fig. 7 in which the "two-step cooling" is clearly indicated by a sudden slope change in the temperature trace. In other words, the material is initially cooled at a relatively slow rate until a certain temperature (200 °C, in the present study) is reached, when the cooling rate is abruptly increased. It should be mentioned that the high-pressure die casting of semi-solid alloys basically consists of two stages: the property-preparation stage and the injection (die-casting) stage. During the former stage, the material in the semi-solid-alloy producer is usually cooled at a much slower rate compared with that during the injection stage. Therefore, a similar temperature change has been intentionally imposed in this type of experiment. However, it should be pointed out that the actual cooling rate occurring in the high-pressure die-casting process could still be one or two orders of magnitude higher than that imposed in the current "fast" cooling stage. The results for the apparent viscocity versus solid fraction (or, equivalently, temperature) for these continuous-cooling experiments will be presented in the next section.

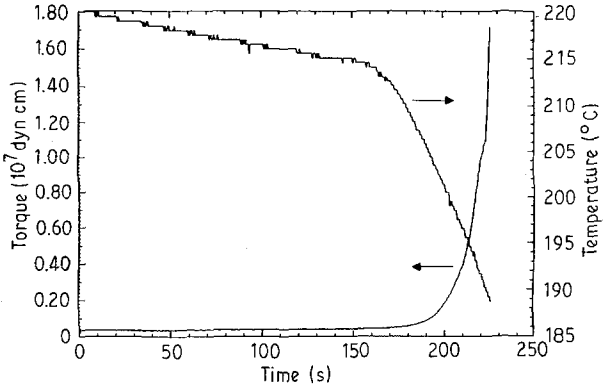

Figure 6 Temperature trace and corresponding torque measurement of semi-solid Sn–15% Pb alloy during fast continuous-cooling experiment with constant shear rate of 675 s^{-1}.

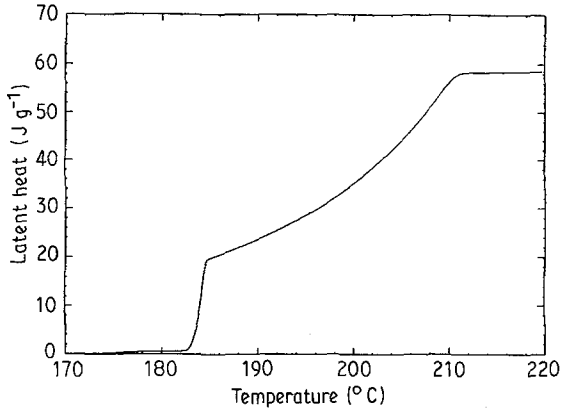

Figure 8 Cumulative latent heat absorbed by Sn–15% Pb alloy during DSC experiment at a scanning rate of 1.25 °C min^{-1}.

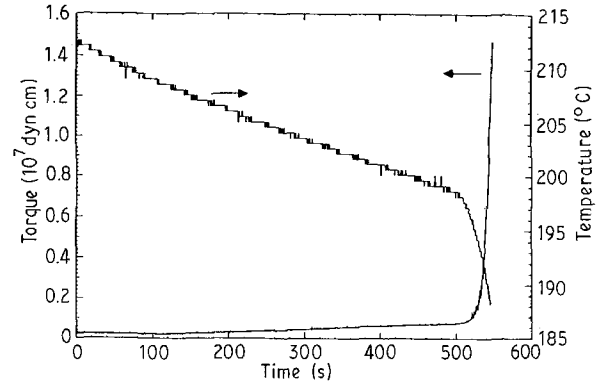

Figure 7 Temperature trace and corresponding torque measurement of semi-solid Sn–15% Pb alloy during two-step cooling experiment with constant shear rate of 450 s^{-1}.

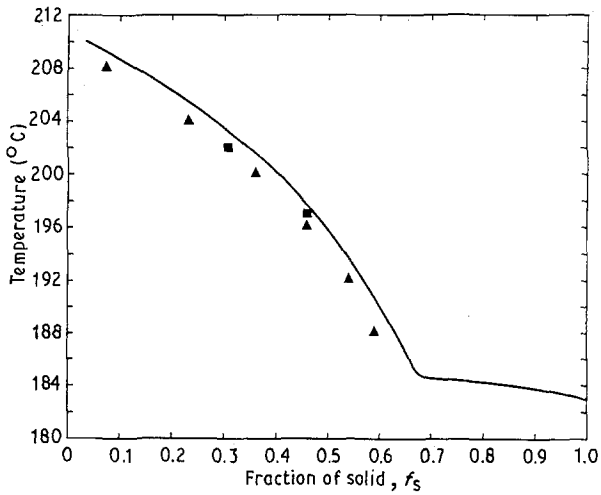

Figure 9 (——) Temperature versus fraction of solid for Sn–15% Pb alloy based upon the results in Fig. 8. (■) Experimental data [18], (▲) calculated solid fraction [18], based upon the Scheil equation and the phase diagram of tin–lead alloy.

2.3. Correlation between fraction of solid and temperature

The majority of previous investigations (see, for example [1–3, 5–11]) have employed either the Scheil equation [16] or the equilibrium lever rule [17] to calculate the weight fraction of solid. Furthermore, by assuming that the density difference between the solid and liquid is negligible (which is true for the Sn–15% Pb alloy [18]), the weight fraction, therefore, can be used to approximate the volume fraction. In the present study, the amount of latent heat absorbed during melting a small sample of Sn–15% Pb alloy at five constant-scanning rates (1.25, 2.5, 5, 10, 20 °C min^{-1}) was measured using a Perkin–Elmer DSC-2C differential scanning calorimeter. It was found that the difference between results at 1.25 and 2.5 °C min^{-1} is negligible. Because the cooling rates employed in the slow-cooling experiments fall within this range, the results at a scanning rate of 1.25 °C min^{-1} were used to calculate the accumulated amount of latent heat absorbed by the sample over the solidification range (cf. Fig. 8). It should be pointed out here that the measured latent heat (58.6 J g^{-1}) agrees very well with results in the literature, such as 58.8 J g^{-1} reported in [18]. Moreover, the solidification range (183–211 °C) indicated in Fig. 8 agrees well with the phase diagram for Sn–Pb alloy in [19]. If one assumes that the accumulated latent heat at some temperature corresponds to the amount of material melted, then a curve correlating temperature with solid fraction can be obtained from Fig. 8 as shown in Fig. 9. Experimental results from Joly [18] obtained by quenching a semi-solid Sn–15% Pb alloy and counting the volume solid fraction through micrographs are also included in Fig. 9. The good agreement indicates that the DSC technique provides an alternative way to determine the solid fraction within the solidification range. Calculated solid fractions from Joly [18] based on the Scheil equation with variable partition ratio are also included in Fig. 9 for comparison.

3. The viscosity model and discussion

3.1. The steady-state viscosity model

In the present study, the isothermal holdings were preset at four temperatures (207, 202, 197, and 192 °C) which, respectively, correspond to solid fractions of 0.17, 0.35, 0.47, and 0.57, based on Fig. 9. Owing to the preferred refined grain structure resulting from high shear rate (at the expense of more power consumption), the initial shear rates employed in this study

varied from 509–1175 s^{-1}. The overall range of shear rate studied, on the other hand, varied from about 200–1750 s^{-1}. Shown in Fig. 10 are log–log plots of the steady-state apparent viscosity versus shear rate at each isothermal stage with their respective solid fraction (f_s) indicated. It is interesting to note that data for the same solid fraction (f_s) tend to cluster together along the same curve regardless of the initial shear rate or the number of isothermal stages employed. However, it should be pointed out that, at a fixed initial shear rate, some of the experiments exhibit a hysteresis loop having a scale smaller than the overall data scattering in Fig. 10 (corresponding to various initial shear rates). Such a phenomenon may be due to small temperature fluctuations during the isothermal-holding stage (cf. Fig. 2) or insufficient dwell time at each fixed shear rate. Another possibility is that the structure of the particles (and/or the particle aggregates) does change slightly with the scanning of shear rate, thereby leading to a change in the steady-state apparent viscosity even when the shear rate returns to the same value.

It can be seen in Fig. 10 that over the shear-rate range of 200–800 s^{-1}, the semi-solid alloy obeys the power-law model, i.e. $\eta = m(f_s)\dot{\gamma}^{-n}$, which has been observed by other investigators [5, 9, 11]. However, when the shear rate exceeds a certain critical value, the apparent viscosity tends to approach an asymptotic value, $\eta_\infty(f_s)$, which, to the authors' knowledge, has never been reported explicitly for semi-solid alloys. This is primarily because the shear rates employed by previous investigators was in a lower range than in the present study. Such shear-thinning behaviour in the power-law region and asymptotic Newtonian trend at higher shear rates could be attributed to the formation and fragmentation of the particle agglomerates. This explanation is based on the well-known fact that solid particles are prone to aggregate through some sort of "welding process" between the particles during collisions. The larger the agglomerate, the more liquid will be entrapped within the agglomerate, thus resulting in a higher effective solid fraction as well as a larger apparent viscosity. However, it seems reasonable that there exists an "equilibrium" size distribution as a function of shear rate (or shear stress), with the agglomerate size decreasing with increasing shear rate. In the limiting case, when the shear rate becomes sufficiently large, no agglomerates exist and each particle becomes an individual entity, thereby leading to an asymptotic constant viscosity. This behaviour can be empirically expressed as

$$\eta(\dot{\gamma}, f_s) = \eta_\infty(f_s)\left[1 + \left(\frac{\dot{\gamma}^*(f_s)}{\dot{\gamma}}\right)^a\right]^{n/a} \quad (1)$$

$$= \eta_\infty(f_s)\left[1 + \left(\frac{\tau^*(f_s)}{\eta_\infty(f_s)\dot{\gamma}}\right)^a\right]^{n/a} \quad (2)$$

with $\eta_\infty(f_s)$, $\dot{\gamma}^*(f_s)$ (or $\tau^*(f_s) \equiv \eta_\infty(f_s)\dot{\gamma}^*(f_s)$), a, and n to be determined by fitting the experimental data, as shown in Fig. 10. In particular, $\dot{\gamma}^*(f_s)$ ($\tau^*(f_s)$) is the critical shear rate (shear stress) which characterizes the transition region between the power-law behaviour (with slope $-n$) and the Newtonian asymptote whereas a characterizes the breath of this transition region. In the present study, the values of n and a have been determined to be 0.93 and 2, respectively, corresponding to the best fit of the current data. Table I lists the values of the asymptotic viscosity, $\eta_\infty(f_s)$, the critical shear rate, $\dot{\gamma}^*(f_s)$, and the critical shear stress, $\tau^*(f_s)$, for the solid fractions studied. It can be seen that the critical shear rate increases with increasing solid fraction. Shown in Fig. 11 are semi-log plots of $\eta_\infty(f_s)$, $\dot{\gamma}^*(f_s)$, and $\tau^*(f_s)$ as functions of solid fraction. It is interesting to note that the functional dependence is approximately exponential for all three parameters and can be expressed as

$$\eta_\infty(f_s) = 0.091\exp(4.32 f_s) \quad (3)$$

$$\dot{\gamma}^*(f_s) = 525\exp(2.35 f_s) \quad (4)$$

$$\tau^*(f_s) = 47.8\exp(6.67 f_s) \quad (5)$$

which correspond to the solid curves in Fig. 11.

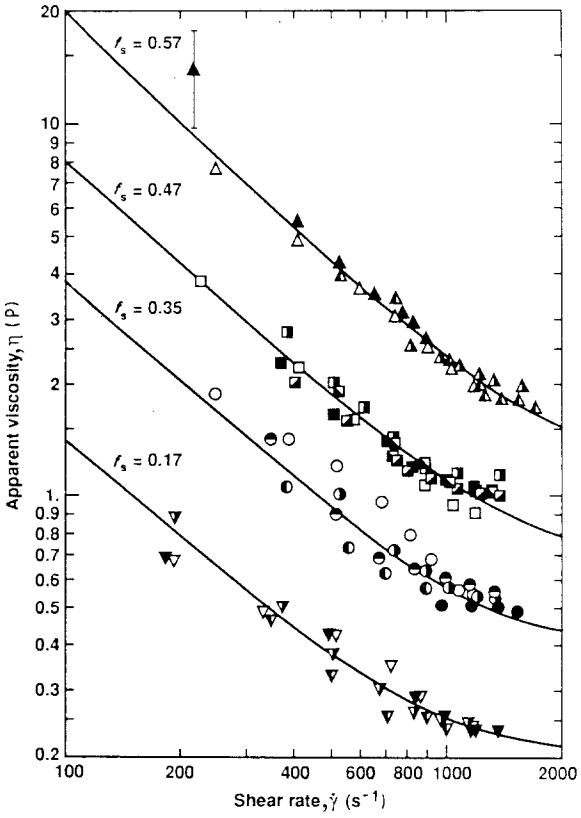

Figure 10 Log–log plot of steady-state apparent viscosity versus shear rate at various solid fractions. Symbols represent experimental data whereas curves are given by Equations 1 and 2 with $n = 0.93$, $a = 2$ and remaining parametric values given in Table I. Initial shear rates (s^{-1}): (▲, ◭, ◮) 509, (▲, ◪) 799, (◬) 803, (△, □, ○, ▽) 1175, (◨, ◐, ▼) 880, (■, ◓, ▼) 821, (●, ▼) 979.

TABLE I Values of asymptotic viscosity, critical shear rate and stress at the fractions of solid studied

	Fraction of solid			
Fraction of solid	0.17	0.35	0.47	0.57
Asymptotic viscosity (P)	0.20	0.39	0.65	1.12
Critical shear rate (s^{-1})	825	1180	1460	2000
Critical shear stress (dyn cm^{-2})	165	460	950	2240

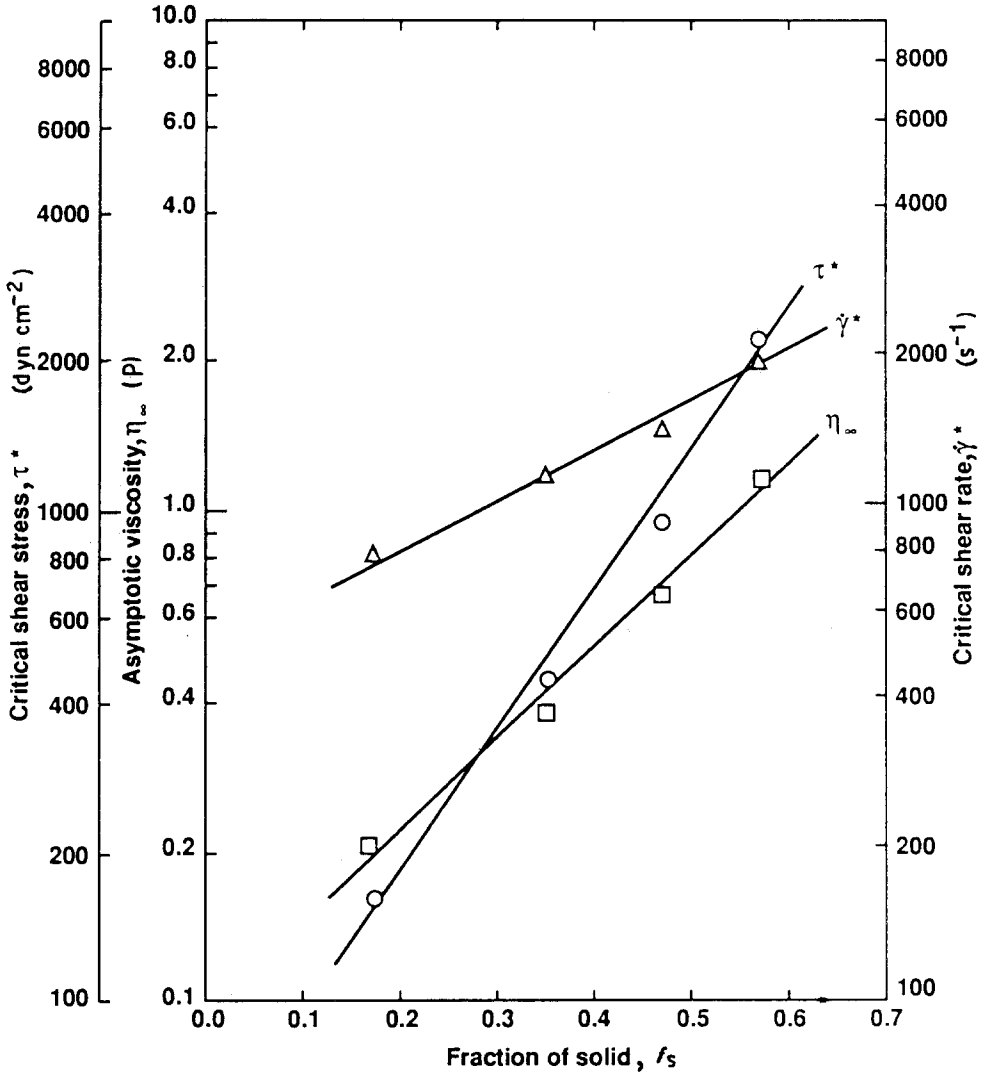

Figure 11 Semi-log plots of asymptotic viscosity, critical shear rate, and critical shear stress as functions of solid fraction.

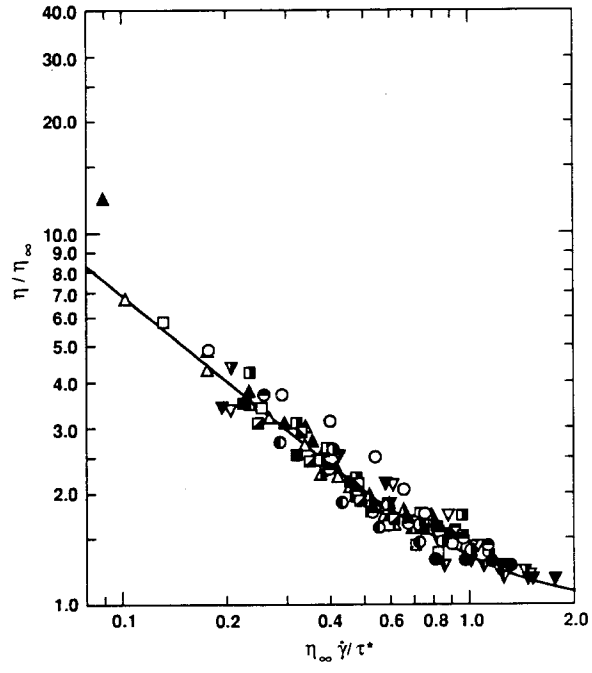

Figure 12 Master plot of the data in Fig. 10 in terms of normalized steady-state apparent viscosity versus normalized shear rate. Solid fraction: triangles, 0.57; squares, 0.47; circles, 0.35; inverted triangles, 0.17. Initial shear rate (s^{-1}): (▲, ◭, ◑) 509, (▲, ◪) 799, (▲) 803, (△, □, ○, ▽) 1175, (◨, ◐, ▼) 880, (■, ◓, ▼) 821, (●, ▼) 979.

As in the case of polymer melts [20], it should be noted that the data in Fig. 10 can be reduced to a master plot (shown in Fig. 12) in terms of η/η_∞ versus $\eta_\infty\dot{\gamma}/\tau^*$ (or $\dot{\gamma}/\dot{\gamma}^*$). Such a master plot not only characterizes the rheological property of this particular semi-solid-alloy system, but also enables one to check the consistency of any additional data with this material.

3.2. Modification of the viscosity model

Shown in Figs 13–17 are the results of apparent viscosity as a function of solid fraction (or temperature), shear rate, and cooling rate for continuously cooled semi-solid Sn-15% Pb alloy corresponding to the slow-, fast-, and two-step cooling experiments at shear rates of 225, 450, 675, 900, and 1125 s^{-1}, respectively. The dashed lines in these figures represent the steady-state apparent viscosity given by Equations 1–5. It can be seen that these steady-state apparent viscosities are generally lower than the data for the continuously cooled sample. Such a discrepancy is probably due to the fact that the structure (and, accordingly, the apparent viscosity) of the semi-solid alloy may change with time, as reflected by its thixotropy discussed elsewhere. In fact, by carefully examining the torque-measurement traces from the

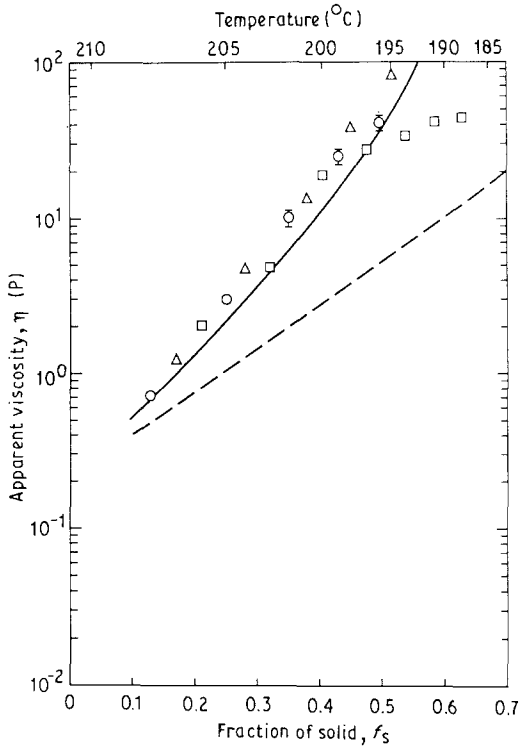

Figure 13 Semi-log plot of apparent viscosity versus solid fraction of continuously cooled semi-solid Sn–15% Pb alloy under a constant shear rate of 225 s^{-1} and various cooling rates (°C min^{-1}): (△) 23.1, (○) 2.1, (□) 2.1/21.0. Steady-state apparent viscosity given by (– – –) Equations 1–5, and (——) Equation 6 with $f_s^* = 0.7$ and $m = 1.6$.

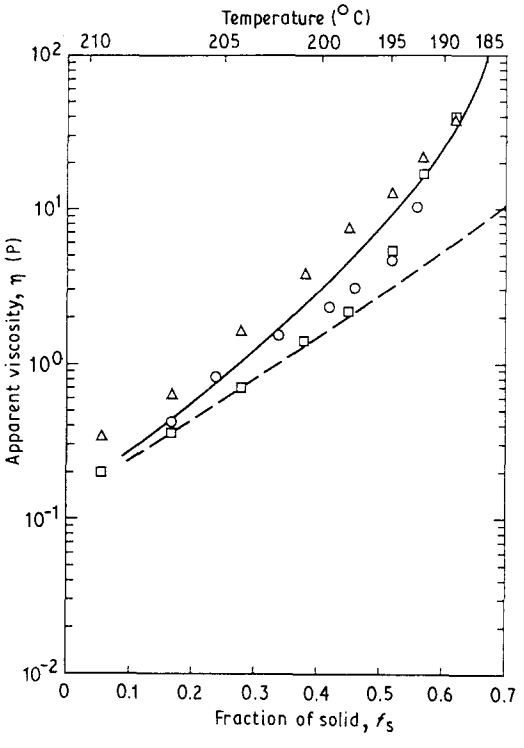

Figure 14 Same as Fig. 13 but at constant shear rate of 450 s^{-1}, $m = 0.8$ in Equation 6, and cooling rates (°C min^{-1}); (△) 25.0, (○) 2.2, (□) 1.7/18.0.

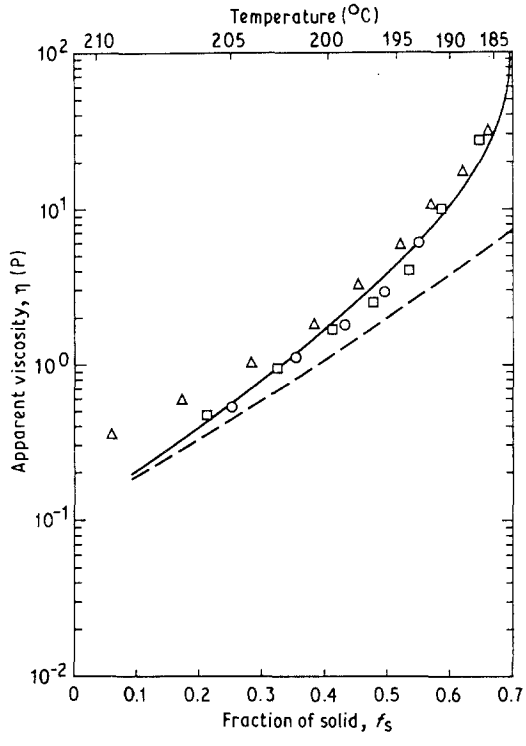

Figure 15 Same as Fig. 13 but at constant shear rate of 675 s^{-1}, $m = 0.53$ in Equation 6, and cooling rates (°C min^{-1}): (△) 28.0, (○) 1.8, (□) 2.0/27.0.

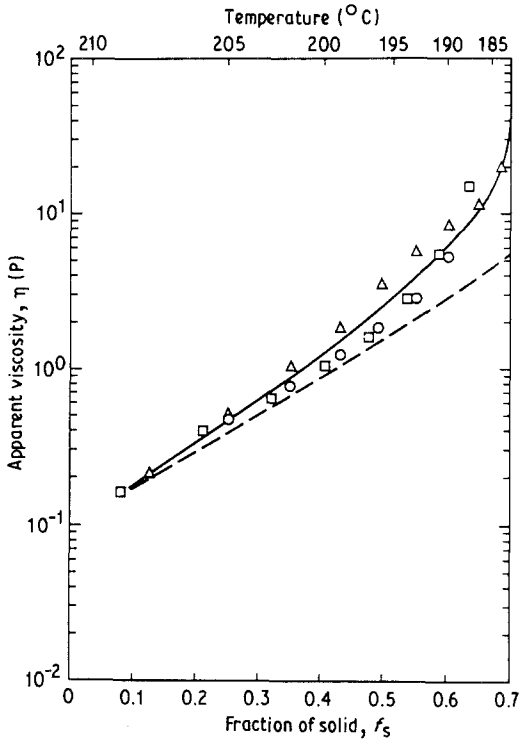

Figure 16 Same as Fig. 13 but at constant shear rate of 900 s^{-1}, $m = 0.4$ in Equation 6, and cooling rates (°C min^{-1}): (△) 25.6, (○) 1.6, (□) 1.7/23.2.

isothermal holding experiments, one can find that the "relaxation time" (i.e. time required for the torque measurement to reach a steady-state value) generally increases with increasing solid fraction or with decreasing shear rate. Relative to the isothermally held sample, the continuously cooled material does not have sufficient time (or, equivalently, enough shear deformation) to reach the steady state, thereby resulting in a higher apparent viscosity (due to more dendritic rather than spherulitic structure as well as more liquid entrapment within the solid phase). This

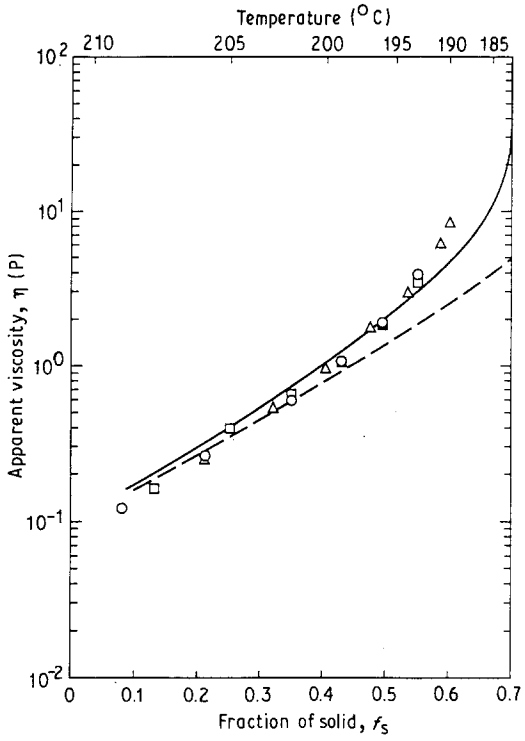

Figure 17 Same as Fig. 13 but at constant shear rate of 1125 s^{-1}, $m = 0.32$ in Equation 6, and cooling rates (°C min^{-1}); (△) 26.0, (○) 2.1, (□) 2.1/22.0.

statement can be justified by the fact that the difference between the viscosity of the continuously cooled sample and the steady-state viscosity is more significant for the cases of low shear rate, fast cooling rate, and high solid fraction, as indicated by the results in Figs 13–17. Also, it should be mentioned that the unusual "levelling off" in the apparent viscosity at high solid fraction for a shear rate of 225 s^{-1} is probably due to the fact that the semi-solid alloy is so viscous that it starts adhering to the surface of the inner cylinder, getting separated from the surface of the outer cylinder due to thermal contraction. Accordingly, the measured viscosity decreases because of the decreasing contact area on the outer cylinder.

Broadly speaking, a higher cooling rate results in a slightly higher apparent viscosity, as shown in these figures. However, it is interesting to note that the apparent viscosities for the slow- and two-step cooling experiments do not differ much at any of the shear rates used. Such a similarity is probably due to the "supercooling phenomenon" which occurs during the fast-cooling stage of the two-step cooling experiment. In other words, the effect of high-cooling rate is somewhat offset by the fact that less solid phase is produced compared to that based upon the nearly equilibrium DSC measurement corresponding to a certain temperature.

In the present study, an additional empirical factor has been incorporated with Equations 1 and 2 to compensate for the discrepancy between the steady-state viscosity and the viscosity of the continuously cooled slurry, resulting in

$$\eta(\dot{\gamma}, f_s) = \left(1 - \frac{f_s}{f_s^*}\right)^{-m(\dot{\gamma})} \eta_\infty(f_s)\left\{1 + \left[\frac{\dot{\gamma}^*(f_s)}{\dot{\gamma}}\right]^a\right\}^{n/a} \quad (6)$$

where $m(\dot{\gamma}) = 360/\dot{\gamma}$ and $f_s^* = 0.7$. The solid curves shown in Figs 13–17 are given by Equation 6. The curves are intended to describe the average trend of all the continuously cooled viscosity data at different cooling rates. By doing so, the effect of cooling rate on the apparent viscosity does not have to be taken into account in the model although the consequent error could be as large as the band width of these transient viscosity data. The reason for doing so is purely for simplicity. However, in actual applications, such as the high-pressure die-casting process, the viscosity variation of the semi-solid alloy is likely to follow the trace of the two-step cooling experiment, as pointed out elsewhere. If that is the case, then a better prediction would be expected by improving the fit of the two-step-cooling experiment. Note that f_s^* in Equation 6 is the critical solid fraction at which the apparent viscosity of the semi-solid Sn–15% Pb alloy goes to infinity. For a suspension system consisting of identical hard spheres, the theoretical value of the critical solid fraction (or the close-packed particle volume fraction) is 74%. In this study, the simple form of the compensating function and the value of the critical solid fraction shown in Equation 6 are chosen in such a way that the model can describe the general trend of the experimental data for all the shear rates employed in the experiments.

As a comparison, Figs 18 and 19 plot the current data for the slow- and fast-cooling experiments, respectively, together with the data of Joly [5] for the same material with the corresponding processing conditions indicated. It can be seen in Fig. 18 that the

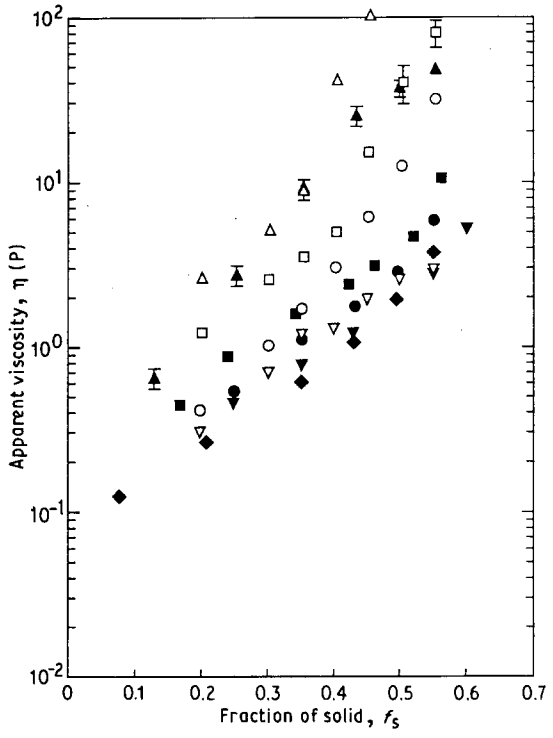

Figure 18 Comparison between current viscosity data (solid symbols) and previous results from [5] (open symbols) at different shear rates indicated for the slow continuous-cooling experiments. Cooling rate (°C min^{-1})/shear rate (s^{-1}): (△) 0.33/115, (□) 0.33/230, (○) 0.33/350, (▽) 0.33/750, (▲) 2.1/225, (■) 2.2/450, (●) 1.8/675, (▼) 1.6/900, (◆) 2.1/1125.

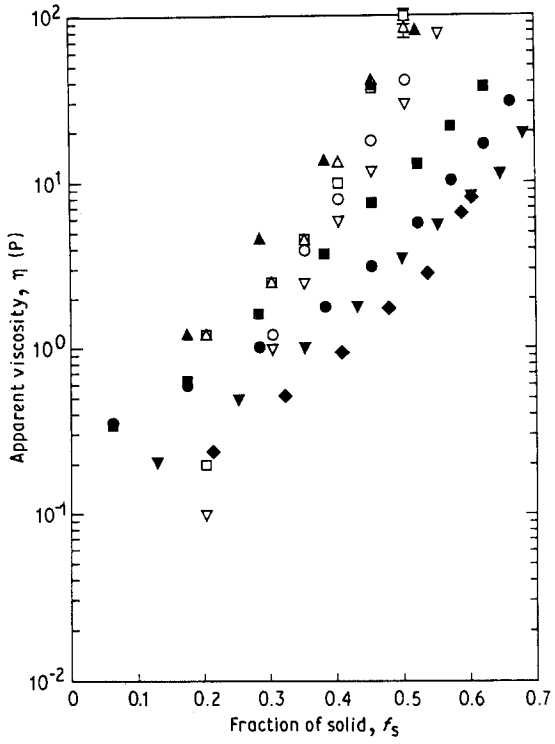

Figure 19 Same as Fig. 18 but for fast continuous-cooling experiments. Cooling rate (°C min^{-1})/shear rate (s^{-1}): (△) 25.0/115, (□) 25.0/230, (○) 25.0/450, (▽) 25.0/750, (▲) 23.1/225, (■) 25.0/450, (●) 28.0/675, (▼) 25.6/900, (◆) 26.0/1125.

present data agree fairly well with the data of Joly at low cooling and shear rates. However, the data for the fast-cooling experiments are somewhat lower than Joly's results at comparable cooling and shear rates (cf. Fig. 19). It should be pointed out that the co-axial cylindrical rheometer used by Joly had a relatively large gap thickness (3 mm as compared to 1.27 mm for the device employed in this study) and had grooves of comparable size over the cylinder surfaces. With such dimensions, a large temperature non-uniformity could easily occur over the thick gap and grooves in the case of fast cooling, thus introducing additional uncertainties. Nevertheless, such a discrepancy evidently warrants further investigation.

Thus far, attention has been focused on situations of either constant temperature (such as that in the isothermal holding experiments) or constant shear rate (such as that in the continuous-cooling experiments). However, in actual practice, as in the high-pressure die-casting process, both temperature and shear rate change continuously during the die-filling stage. Therefore, some of the present two-step cooling experiments have also included variable shear rates in order to investigate further the rheological behaviour of the semi-solid Sn–15% Pb alloy. For example, shown in Fig. 20 are the temperature trace and corresponding torque measurement for one such experiment. It should be noted that the imposed "base shear rate" is held constant (900 s^{-1}) over most of the experiment except during certain periods when the shear rate becomes changed in a kind of sinusoidal manner as reflected by the wiggles in the torque trace. More specifically, each numbered solid symbol in Figs 21a and 22a represents the apparent viscosity at

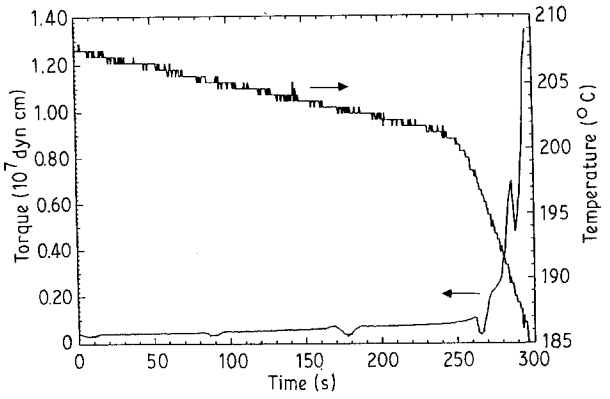

Figure 20 Temperature trace and corresponding torque measurement for semi-solid Sn–15% Pb alloy during two-step cooling experiment with variable shear rate.

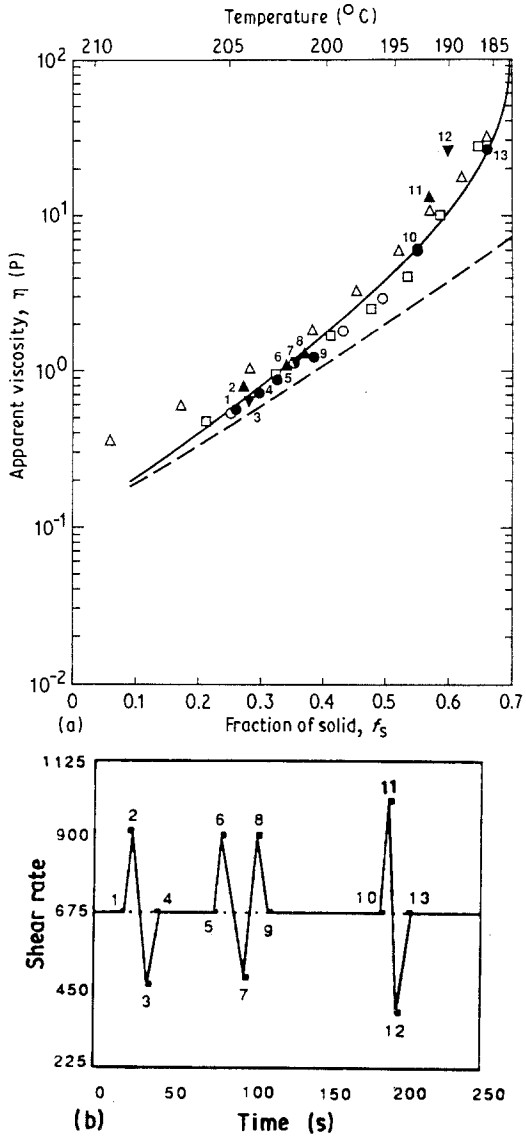

Figure 21 (a) Same plot as Fig. 15 except that the additional numbered solid symbols represent the apparent viscosity at certain points when the shear rate is subject to some kind of sinusoidal variation as shown in (b). The "base shear rate" used for this particular experiment was 675 s^{-1} and the temperature trace was a typical two-step cooling profile. Cooling rate (°C min^{-1}): (△) 28.0, (○) 1.8, (□) 2.0/27.0.

the instant when the shear rate reaches a certain maximum/minimum value in the sinusoidal shear-rate variation as numbered in Figs 21b and 22b. The "base shear rates" used in Figs 21 and 22 are 675 and

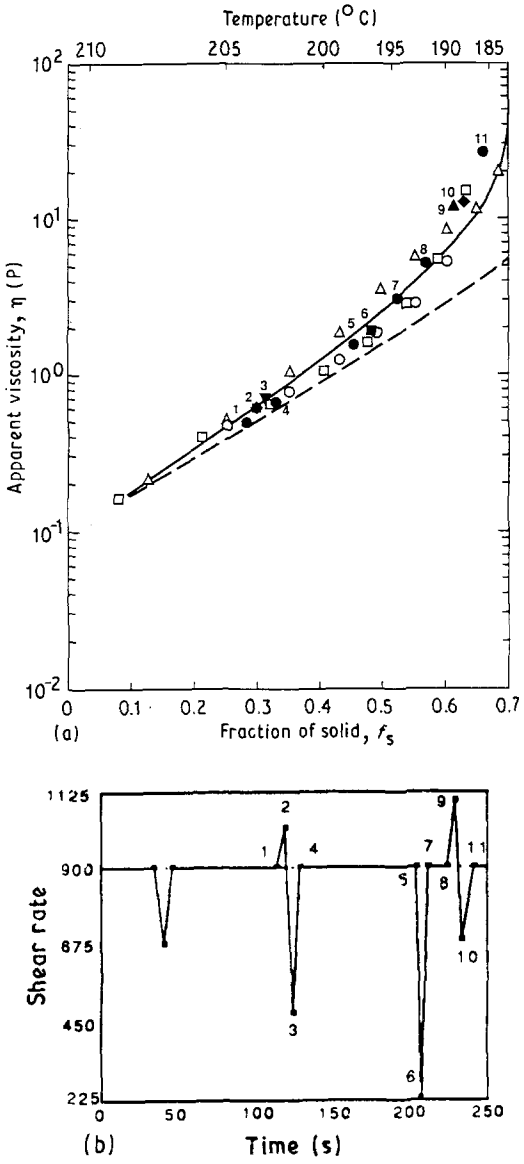

Figure 22 Same as Fig. 21 but related to Fig. 16 with a "base shear rate" of 900 s^{-1}. Cooling rate (°C min^{-1}): (△) 25.6, (○) 1.6, (□) 1.7/23.2.

900 s^{-1}, respectively. For the purpose of comparison, the data points from the constant shear-rate experiments (cf. Figs 15 and 16) corresponding to the present base shear rates are also included as shown by the open symbols. It is interesting to note that the apparent viscosity not only increases with decreasing shear rate, as was found in the isothermal holding experiments, but also increases with increasing shear rate. Such behaviour, which has been found to be repeatable, is opposite to the previous findings with the isothermally held slurry. This opposite trend in viscosity evidently deserves further investigation.

Nevertheless, it can be seen in Figs 21 and 22 that the apparent viscosity only deviates slightly from the trace of the solid curve given by Equation 6 based upon the "base shear rate" with various perturbations in shear rate. In fact, if the time scale (10–20 s) of the shear-rate variation could be made as short as the die-filling time (typically a fraction of 1 s), such deviation in the apparent viscosity would be anticipated to be even smaller. That is, if the semi-solid Sn–15% Pb alloy were prepared under a constant shear rate until a desired solid fraction were reached and the material then immediately used for injection, the subsequent change in viscosity would generally follow the trace corresponding to the "pre-casting" shear rate. Such a conclusion seems to be reasonable in the sense that it is the "pre-casting" shear rate that characterizes the microstructure (and, thus, the apparent viscosity) of the semi-solid alloy before the injection takes place. Once the semi-solid alloy undergoes the quasi quenching-cooling stage (as in the high-pressure die-casting process), the effect of the shear rate should diminish due to the reduced effective shearing time. Therefore, with the aid of the current rheological model, one would be able to produce a semi-solid alloy with desired viscosity by properly choosing the "pre-casting" shear rate as well as the solid fraction. Afterwards, this model could be used to predict the viscosity during the injection stage (when the viscosity now only responds to changes in temperature through its dependence upon f_s) and thus generate useful information for the user to evaluate and/or modify the die design and processing conditions.

Needless to say, the current rheological model still possesses some limitations as a result of the aforementioned idealizations and approximations. However, this represents a first step toward the development of a scientific basis for numerically simulating an innovative die-casting process with semi-solid alloys. As a matter of fact, implementation of the present model into the numerical simulation of a fluidity test for semi-solid alloys has shown very encouraging results as discussed previously [13].

4. Conclusions

The application of semi-solid alloys in the high-pressure die-casting process has inherent advantages over superheated liquid metals. In order to develop the scientific basis for such an innovative die-casting process with semi-solid alloys, a special rheometer system has been designed and fabricated for characterizing the rheology of a semi-solid Sn–15% Pb alloy. A series of experiments has been conducted in a systematic way leading to a rheological model suitable for the mathematical modelling of high-pressure die-casting process. Based on the experimental data, the following conclusions can be drawn.

1. For an isothermally held semi-solid Sn–15% Pb alloy, the apparent viscosity has a power-law behaviour (i.e. $\eta = m(f_s)\dot{\gamma}^{-n}$) over the shear-rate range of 200–800 s^{-1}. However, when the shear rate exceeds a certain critical value $\dot{\gamma}^*(f_s)$, which depends upon the associated solid fraction, f_s, the apparent viscosity tends to approach an asymptotic value, $\eta_\infty(f_s)$. This shear-thinning behaviour in the power-law region and asymptotic Newtonian trend at higher shear rates can be described by Equations 1 and 2 which can be interpreted in terms of a rearrangement of the particle-agglomerate structure which depends upon the shear rate.

2. The apparent viscosity of a continuously cooled Sn–15% Pb alloy is generally higher than that of the isothermal, steady-state apparent viscosity of the same

solid fraction as given by Equations 1–5 regardless of the cooling rates imposed. The difference between these two cases has been found to increase with decreasing shear rate and increasing cooling rate as well as increasing solid fraction. Such a difference is probably due to the fact that the continuously cooled slurry does not undergo as much shear deformation as does the isothermally held semi-solid alloy. In this study, an additional empirical factor has been incorporated into Equations 1 and 2 to compensate for this difference, resulting in Equation 6.

3. Based on experimental results from two-step cooling with variable shear rate, it has been found that the initial shear rate used in preparing the semi-solid alloy during the early slow-cooling stage has a dominant effect on the apparent viscosity over the subsequent fast-cooling stage. In other words, the apparent viscosity of the semi-solid alloy seems to be only a function of the constant "pre-casting" shear rate and temperature (through its dependence upon f_s).

4. Finally, it should be emphasized that the characterization of the rheological properties for a semi-solid Sn–15% Pb alloy will also provide useful material information for modelling other metal-forming processes involving solidification such as sand casting, permanent casting and continuous casting.

Acknowledgements

The authors thank Mr S. P. Wang for performing the DSC measurements, Miss G. Omura for her assistance in some of the experimental work, and Ms T. Howley for preparing some of the figures. This project is supported by the National Science Foundation under the Grant (Grant No. 8815855).

References

1. L. S. TURNG and K. K. WANG, in "Transactions of the 15th International Die Casting Congress", Paper G-T89-043 (North American Die Casting Association, 1989).
2. S. A. METZ and M. C. FLEMINGS, *AFS Trans.* **78** (1970) 453.
3. D. B. SPENCER, R. MEHRABIAN and M. C. FLEMINGS, *Metall. Trans.* **3** (1972) 1925.
4. M. N. GALKIN and S. V. LOMAZOV, *Russ. Casting Prod.* (May 1970) 241.
5. P. A. JOLY and R. MEHRABIAN, *J. Mater. Sci.* **11** (1976) 1393.
6. S. D. E. RAMATI, G. J. ABBASCHIAN and R. MEHRABIAN, *Metall. Trans.* **9B** (1978) 241.
7. B. C. PAI and H. JONES, in "Proceedings of International Conference on Solidification Technique in the Foundry and Cast House", September 1980 (The Metal Society, London, 1983) p. 126.
8. V. LAXMANAN and M. C. FLEMINGS, *Metall. Trans.* **11A** (1980) 1927.
9. H. LEHUY, J. MASOUNAVE and J. BLAIN, *J. Mater. Sci.* **20** (1985) 105.
10. K. ICHIKAWA, S. ISHIZUKA and Y. KINOSHITA, *Trans. Jpn Inst. Metals* **29** (1988) 598.
11. M. A. TAHA, N. A. EL-MAHALLAWY, and A. M. ASSAR, *J. Mater. Sci.* **23** (1988) 1385.
12. A. M. ASSAR, N. A. EL-MAHALLAWY and M.A. TAHA, *Aluminum* **57** (1981) 807.
13. L. S. TURNG, PhD thesis, Cornell University (1990).
14. M. MOONEY and R. H. EWART, *Physics* **5** (1934) 350.
15. J. F. BRADY and G. BOSSIS, *Ann. Rev. Fluid Mech.* **20** (1988) 111.
16. E. SCHEIL, *Z. Metallkde* (1942) 70.
17. M. C. FLEMINGS, in "Solidification Processing" (McGraw-Hill, New York, 1974) p. 34.
18. P. A. JOLY, PhD thesis, Massachusetts Institute of Technology (1974).
19. "Metals Handbook", Vol. 5, "Metallography, Structures and Phase Diagrams", 8th Edn (American Society for Metals, 1973).
20. C. A. HIEBER, in "Injection and Compression Molding Fundamentals", edited by A. I. Isayev (Marcel Dekker, 1987) Ch. 1.

Received 11 January
and accepted 2 August 1990